Atmos. Meas. Tech., 9, 3567–3576, 2016
www.atmos-meas-tech.net/9/3567/2016/
doi:10.5194/amt-9-3567-2016

Atmospheric Measurement Techniques
Open Access

Satellite observation of atmospheric methane: intercomparison between AIRS and GOSAT TANSO-FTS retrievals

Mingmin Zou[1], Xiaozhen Xiong[2,3], Naoko Saitoh[4], Juying Warner[5], Ying Zhang[1], Liangfu Chen[1], Fuzhong Weng[3], and Meng Fan[1]

[1]The State Key Laboratory of Remote Sensing Science, Institute of Remote Sensing and Digital Earth, Chinese Academy of Sciences, Beijing 100101, China
[2]Earth Resources Technology, Inc., Laurel, MD, USA
[3]NOAA Center for Satellite Applications and Research, College Park, MD 20740, USA
[4]Center for Environmental Remote Sensing, Chiba University, 1–33 Yayoi-cho, Inage-ku, Chiba, Japan
[5]Department of Atmospheric and Oceanic Science, University of Maryland, College Park, MD 20740, USA

Correspondence to: Meng Fan (fanmeng@radi.ac.cn) and Ying Zhang (zhangying01@radi.ac.cn)

Received: 10 August 2015 – Published in Atmos. Meas. Tech. Discuss.: 14 October 2015
Revised: 5 July 2016 – Accepted: 11 July 2016 – Published: 3 August 2016

Abstract. Space-borne observations of atmospheric methane (CH_4) have been made using the Atmospheric Infrared Sounder (AIRS) on the EOS/Aqua satellite since August 2002 and the Thermal and Near-infrared Sensor for Carbon Observation Fourier Transform Spectrometer (TANSO-FTS) on the Greenhouse Gases Observing Satellite (GOSAT) since April 2009. This study compared the GOSAT TANSO-FTS thermal infrared (TIR) version 1.0 CH_4 product with the collocated AIRS version 6 CH_4 product using data from 1 August 2010 to 30 June 2012, including the CH_4 mixing ratios and the total column amounts. The results show that at 300–600 hPa, where both AIRS and GOSAT-TIR CH_4 have peak sensitivities, they agree very well, but GOSAT-TIR retrievals tend to be higher than AIRS in layer 200–300 hPa. At 300 hPa the CH_4 mixing ratio from GOSAT-TIR is, on average, 10.3 ± 31.8 ppbv higher than that from AIRS, and at 600 hPa GOSAT-TIR retrieved CH_4 is -16.2 ± 25.7 ppbv lower than AIRS CH_4. Comparison of the total column amount of CH_4 shows that GOSAT-TIR agrees with AIRS to within 1 % in the mid-latitude regions of the Southern Hemisphere and in the tropics. In the mid to high latitudes in the Northern Hemisphere, comparison shows that GOSAT-TIR is $\sim$ 1–2 % lower than AIRS, and in the high-latitude regions of the Southern Hemisphere the difference of GOSAT from AIRS varies from -3 % in October to $+2$ % in July. The difference between AIRS and GOSAT TANSO-FTS retrievals is mainly due to the difference in retrieval algorithms and instruments themselves, and the larger difference in the high-latitude regions is associated with the low information content and small degrees of freedom of the retrieval. The degrees of freedom of GOSAT-TIR retrievals are lower than that of AIRS, which also indicates that the constraint in GOSAT-TIR retrievals may be too strong. From the good correlation between AIRS and GOSAT-TIR retrievals and the seasonal variation they observed, we are confident that the thermal infrared measurements from AIRS and GOSAT-TIR can provide valuable information to capture the spatial and temporal variation of CH_4, especially in the mid-upper troposphere, in most periods and regions.

1 Introduction

As the third most important greenhouse gas after carbon dioxide (CO_2) and water vapor, atmospheric methane (CH_4) has a lifetime of about 12 years and is more effective in absorbing long-wave radiation, as its radiative forcing is about 26 times more than that of CO_2 on a 100-year time horizon and accounts for 32 % of the total anthropogenic well-mixed greenhouse gas radiative forcing (IPCC, 2013). Mainly due to the impact of human activities, the concentration of CH_4 in the atmosphere has increased from the pre-industrial levels of about 700 ppb to recent levels of about 1800–1900 ppb.

Published by Copernicus Publications on behalf of the European Geosciences Union.

Ground-based networks, such as NOAA/ESRL/GMD (National Oceanic and Atmospheric Administration, Earth System Research Laboratory, Global Monitoring Division), provide measurements of CH_4 at the surface with a long temporal record but for a limited number of stations, primarily in the Northern Hemisphere. Aircraft measurements from NOAA/ESRL/GMD (Tans, 2009) and ARIES operated on UK FAAM aircraft (Illingworth et al., 2014), as well as some research campaigns, provide sparse, intermittent measurements of CH_4 vertical profiles. Because of a limited number of in situ measurements in time and space domain, the quantification of CH_4 emissions from different sources and in different regions still remains largely uncertain. In recent years, space-borne measurements of CH_4 from satellites have become available, such as the measurements using the thermal infrared (TIR) sensors, which include the Atmospheric InfraRed Sounder (AIRS) on NASA/Aqua (Aumann et al., 2003; Xiong et al., 2008, 2010a, b), the Tropospheric Emission Spectrometer (TES) on NASA/Aura (Payne et al., 2009; Wecht et al., 2012; Worden et al., 2012), and the Infrared Atmospheric Sounding Interferometer (IASI) on METOP-A and METOP-B (Xiong et al., 2013; Crevoisiter et al., 2009, 2013; Razavi et al., 2009). Measurements using the Near-Infrared (NIR) sensors include the SCanning Imaging Absorption spectroMeter for Atmospheric CHartographY (SCIAMACHY) instrument onboard ENVISAT for 2003–2009 (Frankenberg et al., 2008, 2011), and the Thermal And Near infrared Sensor for carbon Observation (TANSO) onboard the Greenhouse gases Observation SATellite (GOSAT) from 2009 to present (Yokota et al., 2009; Paker et al., 2011; Schepers et al., 2012; Saitoh et al., 2012). These space-borne measurements provide complementary data sources to surface observations for monitoring atmospheric CH_4 with a large spatial and temporal coverage.

AIRS, GOSAT TANSO-FTS TIR and other thermal infrared sensors, including TES and IASI, have been used to retrieve atmospheric CH_4, and these data have been used for analyzing the spatial and temporal variation of CH_4, so an intercomparison of these two different products from AIRS and GOSAT will provide useful information to users to better understand the characteristics of these two products. Validation with AIRS V6 CH_4 data was recently made using ~ 1000 aircraft profiles (Xiong et al., 2015), and the results show the mean biases of AIRS CH_4 at layers 343–441 and 441–575 hPa are -0.76 and -0.05 % and the RMSEs are 1.56 and 1.16 %, respectively. Some correlation of the retrieval error with degrees of freedom (DOFs) was also found, and the errors in the spring and in the high northern latitudes are larger than in other seasons or regions. A comparison between the GOSAT TIR methane retrievals with those of AIRS therefore represents an indirect validation of the GOSAT data with in situ measurements. Section 2 provides a brief introduction of these two instruments, their retrieval algorithms and the data used in this study. Section 3 shows the comparison results, which include the comparison of the retrieved profiles, the information content characterized by the DOFs and the averaging kernels from these two instruments. Both the retrieved CH_4 mixing ratios and the total column amounts in different seasons and different regions are compared. A summary and conclusion are given in Sect. 4.

2 CH_4 retrievals from AIRS and GOSAT-TIR

2.1 AIRS instrument and the retrieval algorithm description

AIRS on the EOS/Aqua satellite was launched in polar orbit (13:30 LST, ascending node) in May 2002. It has 2378 channels covering 649–1136, 1217–1613 and 2169–2674 cm^{-1} at high spectral resolution ($\lambda/\Delta\lambda = 1200$, $\sim 0.5\,cm^{-1}$) (Aumann et al., 2003), and the noise equivalent differential temperature (NeΔT) at a reference temperature of 250 K ranges from 0.14 K in the 4.2 µm region (the lower tropospheric sounding) to 0.35 K in the 15 µm region (the upper tropospheric sounding). The spatial resolution of AIRS is 13.5 km at nadir, and in a 24 h period, AIRS nominally observes the complete globe twice per day. In order to retrieve CH_4 in both clear and partially cloudy scenes, nine AIRS fields of view (FOVs) within the footprint of the Advanced Microwave Sounding Unit (AMSU) are used to derive a single cloud-cleared radiance spectrum in a field of regard (FOR). The cloud-cleared FOR radiance spectrum is then used to retrieve profiles with a spatial resolution of approximately 45 km (Aumann et al., 2003). The atmospheric temperature profiles, water vapor profiles, surface temperatures and surface emissivity are required as inputs to compute the radiances in the CH_4 absorption band. The differences between the computed radiances and the AIRS measured radiances for clear pixels or the derived cloud-cleared FOR radiances for partially cloudy pixels are used to derive CH_4 profiles based on optimal estimation method. A total of 50–60 CH_4 absorption channels near the 7.66 µm band are selected for the retrievals. The AIRS retrieval algorithm is a sequential retrieval method with multiple steps, in which the temperature and water vapor profiles are retrieved using appropriate channels in previous steps. Thus the quality of the CH_4 retrievals depends on the whole AIRS science team's efforts in improving the temperature and moisture profiles as well as surface temperature and emissivity products. More details of AIRS CH_4 retrievals in its most recent version, i.e., version 6 (V6), can be found in Xiong et al. (2015).

2.2 GOSAT TANSO-FTS TIR and the retrieval algorithm description

GOSAT was launched into a sun-synchronous orbit on 23 January 2009 by an H-IIA launch vehicle. GOSAT is on a 666 km orbit and has a 3-day revisit orbit cycle and a 12-day operation cycle. The local solar time is 13:00 ± 15 min. GOSAT carries two sensors: the TANSO-FTS and the

TANSO-CAI. The IFOV of the TANSO-FTS is 10.5 km in diameter, and that of the TANSO-CAI is 0.5–1.5 km in diameter. TANSO-FTS on board GOSAT makes global observations, including both nadir and off-nadir measurements, of approximately 56 000 ground points every 3 days. TANSO-FTS consists of four spectral bands: Band 1 (0.75–0.78 µm), Band 2 (1.56–1.72 µm), Band 3 (1.92–2.08 µm), and Band 4 (5.5–14.3 µm). The spectra resolution of Band 4 is 0.2 cm^{-1} and its signal-to-noise ratio (SNR) averages approximately 300 at Band 4 for a blackbody temperature of 280 K. (Kuze et al., 2009, 2012; Saitoh et al., 2009). More information on TANSO-FTS TIR and its calibration can be found in Kuze et al. (2012). In the TIR retrieval algorithm version 1.0, all the channels in 7.3–8.8 µm, which include both the CH_4 and N_2O absorption bands, are used for CH_4 retrieval. In the TANSO-FTS TIR V1.0 CH_4 retrieval processing, we simultaneously retrieve H_2O, N_2O, O_3, and temperature other than CH_4. We also simultaneously derive surface temperature and surface emissivity as a correction parameter of spectral bias inherent in TANSO-FTS TIR V161.160 L1B spectra in the same manner as CO_2 retrieval (Saitoh et al., 2016).The retrieval algorithm is a non-linear maximum a posteriori method with linear mapping (Rodgers, 2000). The a priori CH_4 profiles used in the retrieval are taken from the National Institute for Environmental Studies (NIES) transport model (Maksyutov et al., 2008; Saeki et al., 2013). Profiles of temperature and water vapor required for the retrieval are taken from the Japan Meteorological Agency Grid Point Values (JMA-GPV) data set. Values of surface emissivities are estimated by a linear regression analysis using the Advanced Spaceborne Thermal Emission Reflection Radiometer (ASTER) spectral library (Baldridge et al., 2009), the information of land cover, sea ice, wind speed, and the vegetation index derived from the TANSO-Cloud and Aerosol Imager (CAI). Surface temperatures are estimated from the TANSO-FTS TIR spectra in the window region. The signal-to-noise ratios (SNR) of TANSO-FTS at around the 7–8 µm band are estimated to be 70–100, and the measurement covariance matrix used in the retrieval is based on the SNR values. The footprint of GOSAT-TANSO is 10.5 km in diameter, and the number of scan points of GOSAT in cross-track direction is five before July 2010 and three thereafter.

2.3 Data used

This study is made using the standard products of both sensors. GOSAT TANSO-FTS TIR Level 2 CH_4 profile products in version 01.01 for a 2-year period from August 2010 to June 2012 are used, and the data during this period have been released to all registered users selected under the GOSAT research announcement. AIRS V6 CH_4 data are used in this study, and they are downloaded from Goddard Earth Sciences Data and Information Services Center (DISC) (http://mirador.gsfc.nasa.gov/cgi-bin/mirador/presentNavigation.pl?tree=project&project=AIRS). Only

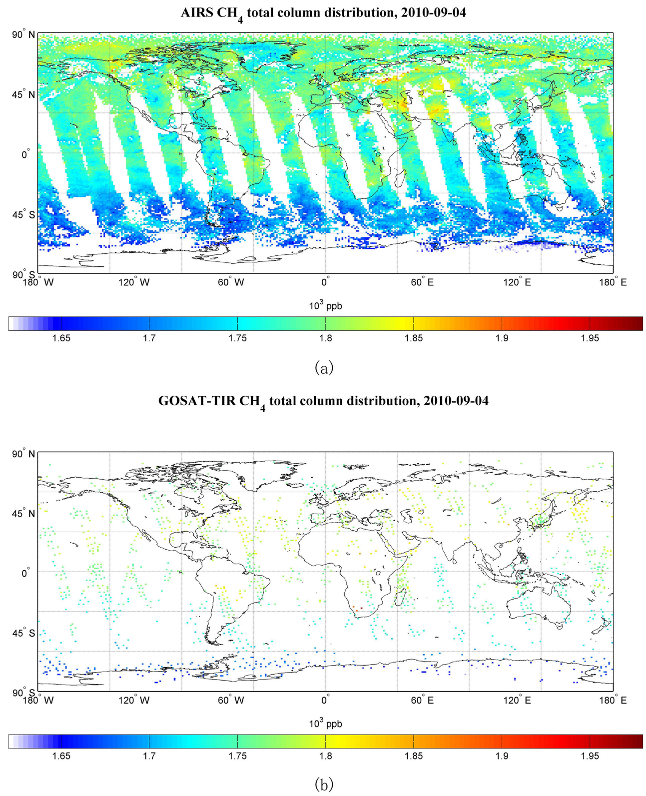

Figure 1. Much larger coverage of AIRS retrievals **(a)** as compared to GOSAT TANSO-FTS **(b)** as shown from the global CH_4 total column density on 4 September 2010. AIRS data from ascending mode with QC = 0, 1 are plotted.

the data from the ascending mode of AIRS, with quality flag equal to 0 or 1, are used for comparison with GOSAT-TIR. Note that the number of retrieval profiles from AIRS is much denser than GOSAT-TIR, as shown in Fig. 1. In this case, the number of profiles from GOSAT-TIR is 1479, while the number of the AIRS profiles from ascending node with QC = 0 and 1 is 164 355. The AIRS retrievals within 1° from each GOSAT-TIR measurement and in the same day were averaged to match up with each GOSAT-TIR measurement. The errors resulting from the time difference of about 4 h between AIRS and GOSAT-TIR observations were not accounted for in this study given that CH_4 is a long-lived and well-mixed gas. For simplification, in the comparison of the total column CH_4, the AIRS gridded products from NASA DISC in 1° × 1° were used directly, and the GOSAT-TIR data were interpolated to the same geographical grid as AIRS.

Comparisons between GOSAT-TIR and AIRS CH_4 products include (1) CH_4 profile comparison, (2) comparison of CH_4 mixing ratios with and without using the averaging kernels, and (3) comparison of the column-averaged CH_4 and the total column abundance in different latitude zones and different times. The CH_4 total column abundance from AIRS

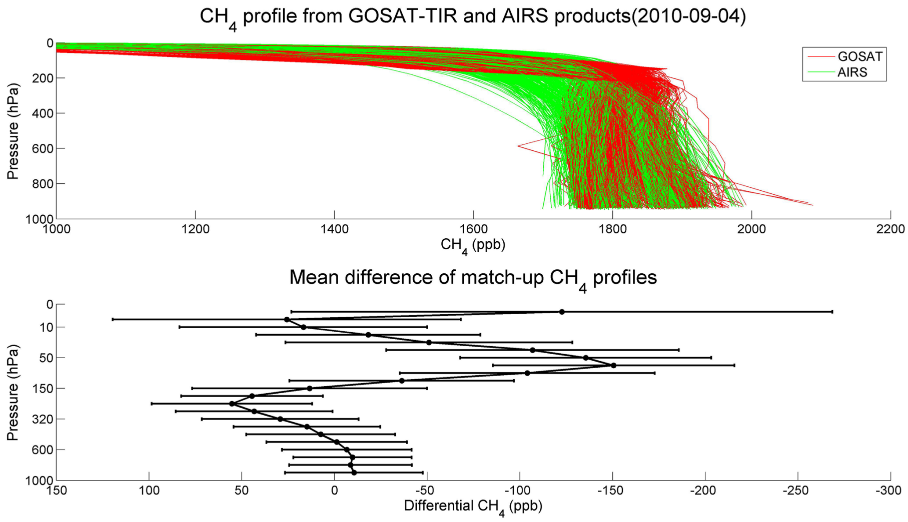

Figure 2. Comparison of the matched-up AIRS CH_4 profiles versus the GOSAT-TIR profiles using 1 day of global data on 4 September 2010. $N = 1182$. Lower panel is the mean difference of AIRS minus GOSAT profiles.

ascending mode whose unit is molecules cm^{-2} was used. Since the unit of GOSAT-TIR CH_4 profile was ppb, pressure profile $\boldsymbol{P}$ and surface pressure P_0 are used to convert the unit of GOSAT-TIR CH_4 profile. First, pressure gradient is calculated as

$$\Delta \boldsymbol{P}_i = \boldsymbol{P}_{i+1} - \boldsymbol{P}_i, \quad (1)$$

where i denotes layer number; the formula to calculate Tc is

$$\mathrm{Tc} = \sum \Delta \boldsymbol{P}_i \cdot \boldsymbol{X}_i / (P_0 - P_\mathrm{T}), \quad (2)$$

where P_T is the top-layer pressure. Pressure profile is included in the GOSAT-TIR product. As a GOSAT TANSO-FTS TIR CH_4 profile consists of 22 layers, and AIRS-V6 CH_4 profile contains 100 layers in the supporting product and 10 layers in the standard product, interpolation of AIRS CH_4 profile from 100 layers to 22 layers was made using the pressure data included in both CH_4 products.

Later in this paper the "differences" between GOSAT-TIR and AIRS CH_4 are calculated as

$$\Delta X = X_\mathrm{G} - X_\mathrm{A}$$
$$\text{Or} \quad (X_\mathrm{G} - X_\mathrm{A})/X_\mathrm{A} \times 100\,\%, \quad (3)$$

where X_G denotes the CH_4 mixing ratios or column amounts from GOSAT-TIR, and X_A from AIRS.

3 Results

3.1 Profile comparison

Figure 2 shows a simple comparison of the GOSAT-TIR profiles and the coincident AIRS CH_4 profiles from 1 day of global data on 4 September 2010. They are in a good agreement above 100 hPa and below 400 hPa, with mean difference no more than 50 ppb, but at 200–300 hPa AIRS CH_4 spans a large range and tends to be smaller than GOSAT TIR on average.

The averaging kernels are defined to provide a characterization of the relationship between the retrieval and the true state. The retrieval sensitivity can be obtained from the sum of the rows of the averaging kernel matrix, which is also referred to as "the area of the averaging kernel" (Rodgers, 2000). To better demonstrate the differences in sensitivities between AIRS and GOSAT-TIR retrievals, Fig. 3 shows an example of the averaging kernels using data at a randomly selected location (38° S, 180° W) on 4 September 2010. There are 10 retrieval layers for AIRS and 22 for GOSAT-TIR. The area of the averaging kernels, which is computed as the sum of all individual kernels, from AIRS is larger than that from GOSAT-TIR, as shown in Fig. 3. To demonstrate the sensitivity variations in latitudes, Fig. 4 shows a curtain plot of the area of averaging kernels using 1 day of global data on 4 September 2010. Overall, the patterns from AIRS are similar to GOSAT TIR, with both peak sensitivities located in the 300–600 hPa range in the high latitudes and 200–600 hPa in the tropics. The sensitivities below 800 hPa are small for both, which reflects the major limitation of TIR in measuring the change of CH_4 in the lower troposphere.

The information content, which is usually represented as the DOF, is computed as the trace of the averaging kernel matrix (Rodgers and Connor, 2003). Figure 5 shows the variation of DOFs at different latitudes, and on average the DOF of AIRS CH_4 is approximately 1.1, whereas the mean DOF for the GOSAT-TIR retrieval of CH_4 is approximately 0.61.

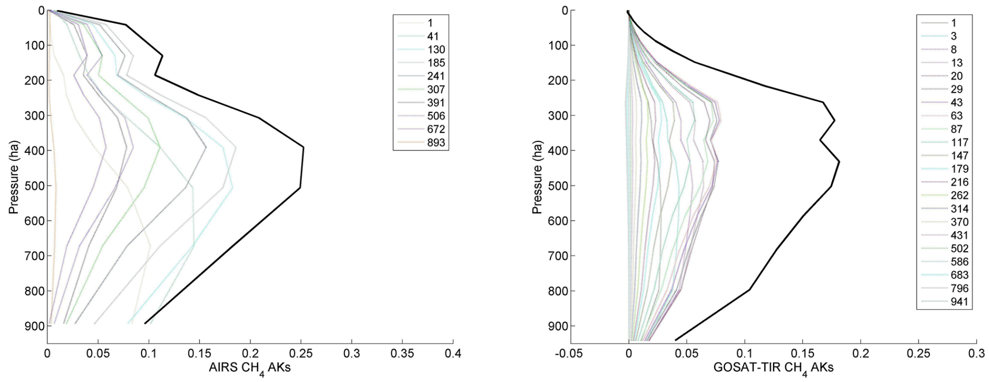

Figure 3. The averaging kernels of AIRS and GOSAT TANSO-FTS TIR V1.0 CH_4 retrievals on 4 September 2010. There are 10 dashed lines for AIRS retrievals and 22 dashed lines for GOSAT retrievals, corresponding to the retrieval layers used in each of them. The black solid line is the area of kernels divided by 4.

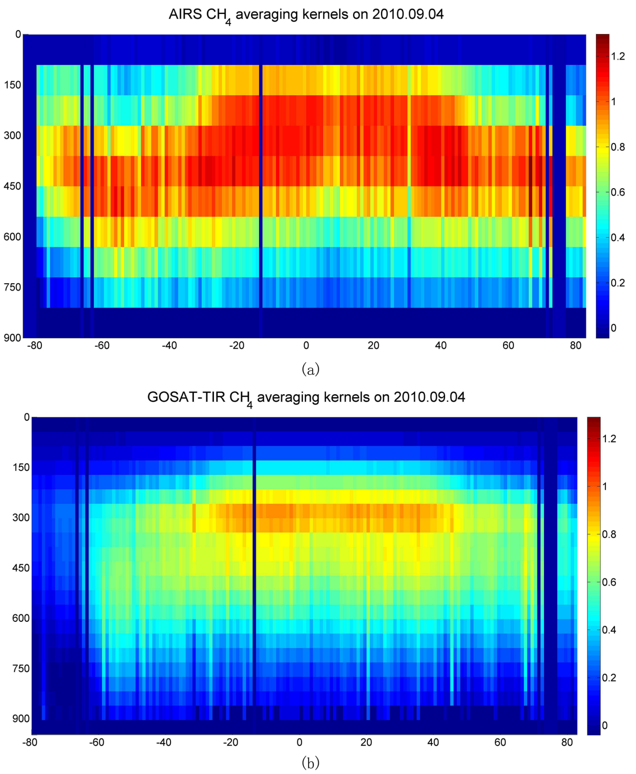

Figure 4. The area of the averaging kernels of CH_4 retrievals from **(a)** AIRS and **(b)** GOSAT TANSO-FTS V1.0 TIR observations at different latitudes on 4 September 2010.

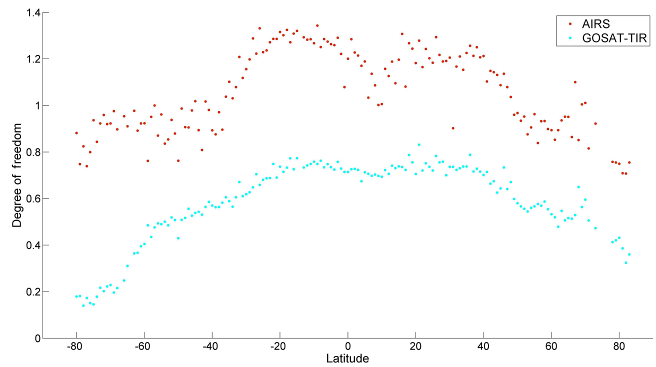

Figure 5. Latitudinal variation of DOF for AIRS and GOSAT TANSO-FTS V1.0 CH_4 retrievals on 4 September 2010.

3.2 Comparison of CH_4 with and without using the averaging kernels

Since intercomparison is made between two space-based sensors, it is necessary to take account of the different characteristics of the observing systems, particularly their averaging kernels, which is usually applied to the "truth" based on the following equation (Rodgers and Connor, 2003):

$$\hat{\boldsymbol{X}} - \boldsymbol{X}_{\mathrm{c}} = \mathbf{A}(\boldsymbol{X} - \boldsymbol{X}_{\mathrm{c}}) + \boldsymbol{\epsilon}_{\mathbf{x}}, \tag{4}$$

where **A** is the averaging kernel. Here we use this equation to calculate the difference between GOSAT-TIR and AIRS CH_4. So $\boldsymbol{X}$ represents the true state of CH_4 profile; $\boldsymbol{X}_{\mathrm{c}}$ is the mean of comparison ensemble of CH_4 profile, and it can be calculated using a regression-based function of latitude and longitude; $\hat{\boldsymbol{X}}$ is the retrieved quantity related to the true profile $\boldsymbol{X}$ and $\boldsymbol{\epsilon}_x$ is the error. The computed value of $\hat{\boldsymbol{X}}$ is referred to as the convolved data later in this paper, which is usually compared with the retrieved CH_4 mixing ratio in validation studies. Considering that the AIRS retrieval layers are coarser than those of GOSAT-TIR, we used the AIRS averaging kernels, **A**, to convert the GOSAT-TIR CH_4 profiles, $\boldsymbol{X}$, and the convolved (or smoothed) GOSAT-TIR profiles ($\hat{\boldsymbol{X}}$) are then used to derive CH_4 total column for comparison. This calculation is based on the Eq. (25) from Rodgers and Connor (2003).

$$\hat{c_{12}} = c_{\mathrm{c}} + \boldsymbol{a}_1^{\mathbf{T}}(\hat{\boldsymbol{X}} - \boldsymbol{X}_{\mathrm{c}}), \tag{5}$$

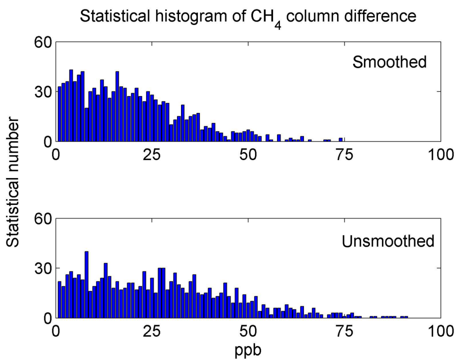

Figure 6. Comparison of AIRS and GOSAT-TIR CH_4 matched-pair difference. The upper panel shows the statistical histogram of AIRS CH_4 difference to smoothed GOSAT-TIR CH_4 and the lower panel shows that to unsmoothed GOSAT-TIR CH_4.

where $\boldsymbol{a}_1$ is the total column averaging kernel of AIRS CH_4; c_c is the total column derived from $\boldsymbol{X}_c$; and $\hat{c_{12}}$ is the related total column using convolved GOSAT-TIR profiles. As the AIRS averaging kernel is a 10 by 10 matrix, the GOSAT-TIR CH_4 profile and AIRS first-guess profile are interpolated onto the 10 pressure layers of the AIRS retrieval grid.

Figure 6 shows the distribution of the absolute differences between GOSAT-TIR CH_4 and AIRS CH_4 column mixing ratios. The upper panel gives the statistical histogram of AIRS CH_4 difference to smoothed GOSAT-TIR CH_4, while the lower panel shows that to unsmoothed GOSAT-TIR CH_4. According to Fig. 6, the number of matched pairs with small differences increases after smoothing. A comparison of the column-averaged mixing ratio, X_{CH_4}, in Fig. 7 also shows that the correlation coefficient between AIRS and GOSAT TANSO-FTS TIR retrievals increases from 0.88 to 0.91 after using the smoothed data, and the mean difference decreases from −21.32 to −2.78 ppb. The mean difference and standard deviation between AIRS and the smoothed GOSAT-TIR data are smaller than those without smoothing using the averaging kernels, demonstrating that applying the averaging kernels helps achieve better agreements in the intercomparison between two different measurements, as suggested by Rogers and Connor (2003).

To show the impact of using averaging kernels in the intercomparison, Fig. 8 shows the scatter plot of AIRS versus GOSAT-TIR CH_4 mixing ratios in four retrieval layers of 272–343, 343–441, 441–575 and 575–777 hPa. The correlation coefficients between AIRS and the smoothed GOSAT-TIR values are 0.70, 0.70, 0.79 and 0.87 in these four layers respectively, while the correlation coefficients between AIRS and GOSAT-TIR without smoothing are 0.36, 0.45, 0.57 and 0.75 respectively.

In next sections, we will focus on the comparison of the total abundance between AIRS and GOSAT-TIR retrievals without applying averaging kernel for smoothing.

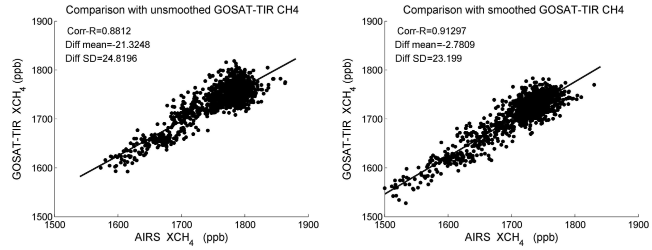

Figure 7. Comparison of X_{CH_4} between AIRS and **(a)** unsmoothed GOSAT TANSO-FTS TIR X_{CH_4} and **(b)** smoothed GOSAT-TIR X_{CH_4} using AIRS averaging kernel. Global data on 4 September 2010 are used.

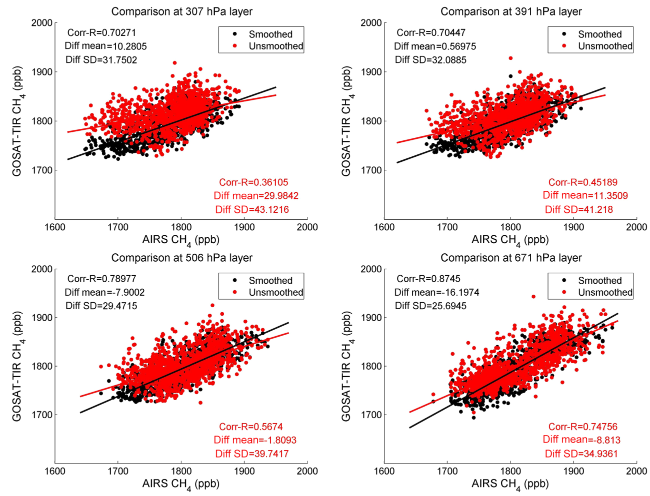

Figure 8. Comparisons of AIRS and GOSAT TANSO-FTS TIR smoothed CH_4 at four retrieval pressure levels of 272–343 hPa, 343–441 hPa, 441–575 hPa and 575–777 hPa (the mean effective pressures are 307, 391, 506 and 671 hPa respectively) using 1 day of data on 4 September 2010.

3.3 Comparison of CH_4 total column abundance in different latitude zones

As the sensitivity of TIR measurements is impacted by the surface thermal contrast and the water vapor content in the atmosphere (Deeter et al., 2007; Xiong et al., 2010b), the sensitivity varies with latitudes and seasons. Below we compare the differences between AIRS and GOSAT TANSO-FTS TIR retrieved total column abundance in six latitude zones from south to north with an interval of 30°. As shown in Figs. 9 and 10, the correlations between AIRS and GOSAT-TIR are reasonably good, and the correlation coefficient for the least correlated case is 0.83 in zone 30–60° S. The split of CH_4 daily comparison is due to these data being located in the high mountains between Chile and Bolivia in South America. This reflects a larger uncertainty in the mountain or coastline regions for AIRS and/or GOSAT. To show the change of their differences with time, Figs. 9 and 10 also show the monthly

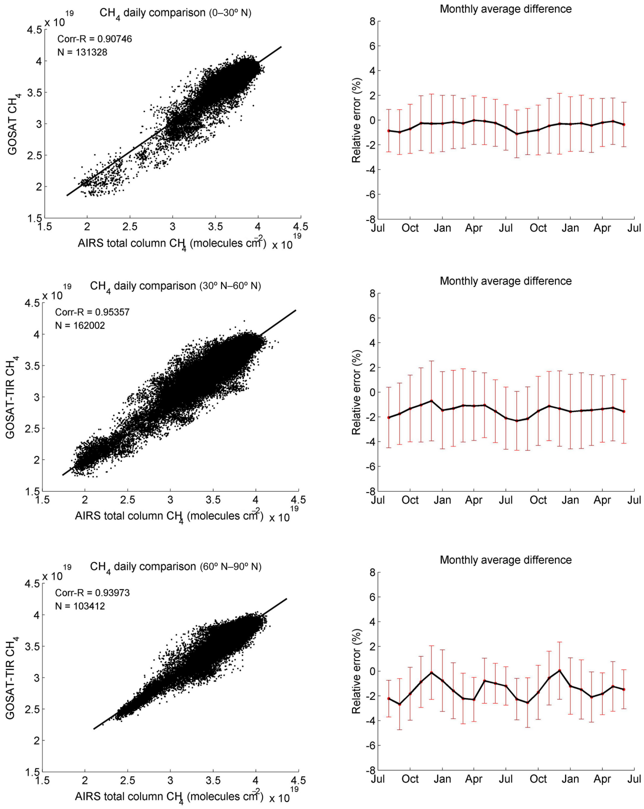

Figure 9. Scatter plot of AIRS versus GOSAT TANSO-FTS TIR CH_4 total column density over three latitude zones in the Northern Hemisphere using data from 1 August 2010 to 30 June 2012 (left panels). Right panels show the variation of the mean difference in each month, and the bars are the standard deviation.

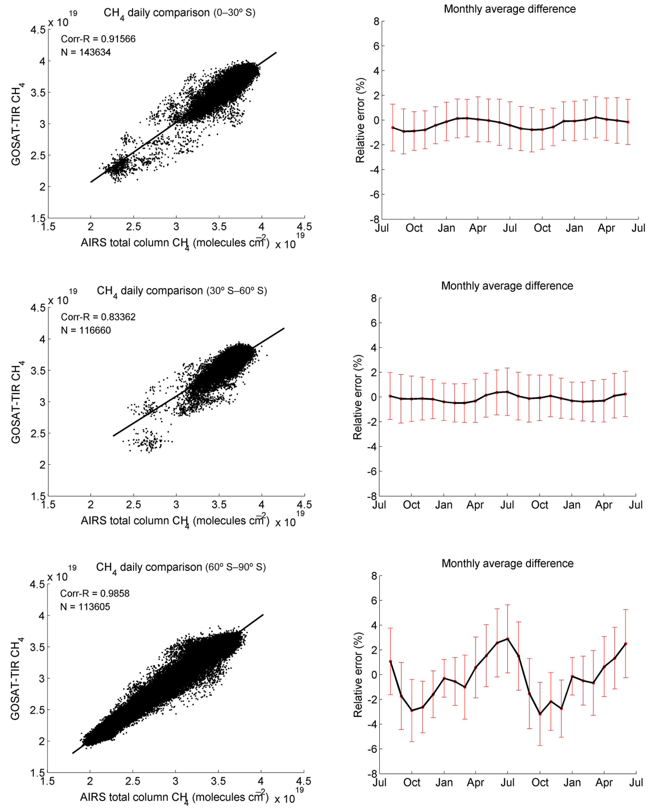

Figure 10. Same as Fig. 8 but for three latitude zones in the Southern Hemisphere.

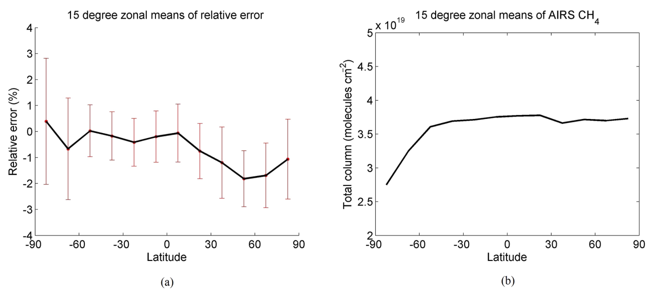

Figure 11. (a) Means of relative errors of GOSAT-TIR total column CH_4 relative to AIRS total column CH_4 in every 15° zonal using data from 1 August 2010 to 30 June 2012. (b) 15° zonal means of AIRS CH_4 total column.

means of the differences from August 2010 to June 2012. In the tropics their differences are less than 1 % in all seasons, but in the mid to high latitudes in the Northern Hemisphere, GOSAT-TIR is ∼ 1–2 % lower than AIRS, with the largest bias occurring in September. At high latitudes in the Southern Hemisphere (60–90° S) the differences of GOSAT from AIRS show a large variation with time, i.e., from −3 % in October to +2 % in July. This large difference in the high attitudes in the Southern Hemisphere is related to the very low DOFs, particularly in GOSAT-TIR retrievals (see Fig. 5), and the large uncertainties in the retrieval of atmospheric states when there is snow/ice coverage over the ocean during October to July.

To better show the difference between GOSAT-TIR and AIRS in different latitudes, we computed the mean difference over a 2-year period from 1 August 2010 to 30 June 2012 and in each 15° zone. As shown in Fig. 11, the standard deviations in the Southern Hemisphere high latitudes are much larger than in the other latitudes, and the mean differences are smaller from 60° S to 10° N but increase in the Northern Hemisphere to −1.5 % at 60° N.

3.4 Comparison of seasonal cycles from AIRS and GOSAT

Using the monthly averaged total column density of CH_4 from AIRS and GOSAT products, we compared the seasonal cycles of CH_4 from 1 August 2010 to 30 June 2012. The left panels in Fig. 12 are the comparisons in the Northern Hemisphere, and the right panels are the comparisons in the Southern Hemisphere. Again, GOSAT-TIR agrees with AIRS to within 1 % in the mid-latitude regions of the Southern Hemi-

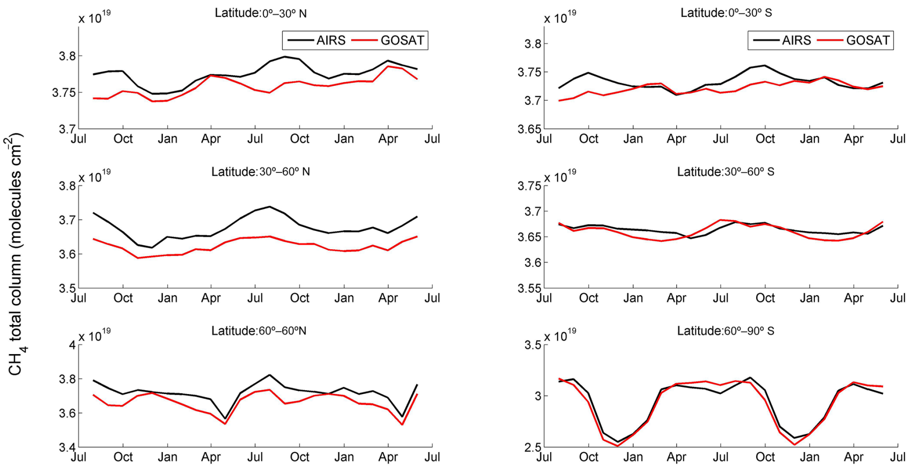

Figure 12. Trends of CH_4 monthly averaged total column amounts in different latitudes using AIRS and GOSAT-TIR products from 1 August 2010 to 30 June 2012. The left panels are the comparison in the Northern Hemisphere and the right panels are the comparison in the Southern Hemisphere.

sphere and in the tropics. However, the seasonal variation in the tropics from AIRS observations is larger than that from GOSAT. In the mid to high latitudes in the Northern Hemisphere, GOSAT-TIR is $\sim$ 1–2 % lower than AIRS, but the seasonal variations agree well. In the high-latitude regions in the Southern Hemisphere, the seasonal variation of the total column of CH_4 is large, which is due to a lot of data points with very low total column of CH_4 observed during October–January from both AIRS and GOSAT-TIR. However, AIRS and GOSAT agree well in capturing the variation even though their difference is relatively larger than in other regions (see Fig. 10).

4 Summary and conclusions

A thorough comparison of AIRS V6 and GOSAT TANSO-FTS TIR V1.0 CH_4 products using 2 years of data (1 August 2010 to 30 June 2012) has been made. In this comparison, AIRS measurements within a collocation window of 1° by 1° from each GOSAT-TIR measurement in the same day were used. Both the CH_4 mixing ratios and total column amounts have been compared. To understand the differences in the retrievals from these two different instruments, we also compared the differences in the averaging kernels and the DOFs and examined the use of averaging kernels on the comparison results.

The peak sensitive layers of AIRS and GOSAT-TIR are at similar height, which is at 200–600 hPa in the tropics and 300–600 hPa in the high-latitude regions. However, due to the lower SNR of GOSAT TANSO-FTS spectra in the 7–8 µm CH_4 band, or over-constraint in the GOSAT retrieval algorithm, the DOF of GOSAT-TIR V1.0 retrievals is lower than AIRS.

The comparisons of the profiles showed that the AIRS CH_4 is similar to GOSAT-TIR CH_4, except that the AIRS values tend to be lower than GOSAT-TIR at 200–300 hPa. At 300 hPa, the CH_4 mixing ratios from GOSAT are 10.3 ± 31.8 ppbv higher than AIRS, and at 600 hPa, the GOSAT-TIR CH_4 is -16.2 ± 25.7 ppb lower than AIRS. Between 300 and 600 hPa, where they have peak sensitivities, AIRS and GOSAT-TIR agree very well. As expected, applying the averaging kernels to smooth the GOSAT-TIR retrievals results in a better agreement between GOSAT with AIRS products.

The comparison of the total column amounts of CH_4 shows that the correlation coefficients between AIRS and GOSAT TANSO-FTS TIR are more than 0.8 in all cases, and the GOSAT-TIR CH_4 agrees with AIRS to within 1 % in the mid-latitudes of the Southern Hemisphere and tropics, but in the mid to high latitudes of the Northern Hemisphere, GOSAT-TIR is $\sim$ 1–2 % lower than AIRS depending on different seasons. In the high latitudes of the Southern Hemisphere the bias varies from -3 % in October to $+2$ % in July. This large difference in high-latitude regions is associated with the low information content (or DOFs) and larger uncertainties in the retrievals of both AIRS (Xiong et al., 2015) and GOSAT. Thus a much stricter quality control should be used as suggested by Xiong et al. (2015). We also found AIRS and GOSAT-TIR have a good agreement in capturing the monthly variation of CH_4 density.

In this study, the time difference between AIRS and GOSAT-TIR measurements has not been taken into account. So, the differences, if they could have been measured at the same time, could be slightly smaller than what we presented here. These results demonstrate that the thermal infrared sensors such as AIRS and GOSAT TANSO-FTS TIR can provide valuable consistent information of CH_4 in the mid-upper troposphere. Further comparisons using more recent data as well as direct comparison with aircraft measurements are ongoing.

5 Data availability

The data set of AIRS V6 CH_4 product used in this study is available at Goddard Earth Sciences Data and Information Services Center (DISC) (http://mirador.gsfc.nasa.gov/cgi-bin/mirador/presentNavigation.pl?tree=project&project=AIRS). And the GOSAT TANSO-FTS TIR Level 2 CH_4 product can be freely download at GOSAT user interface gateway (GUIG) (https://data.gosat.nies.go.jp/GosatUserInterfaceGateway/guig/GuigPage/open.do).

Acknowledgements. This work was supported by the Key Program of the National Natural Science Foundation of China (no. 41130528), National Natural Science Foundation of China (nos. 41401387 and 41201353). This study was performed within the framework of the GOSAT Research Announcement.

Edited by: J. Worden
Reviewed by: three anonymous referees

References

Aumann, H. H., Chahine, M. T., Gautier, C., Goldberg, M. D., Kalnay, E., McMillin, L. M., Revercomb, H., Rosenkranz, P. W., Smith, W. L., Staelin, D. H., Strow, L. L., and Susskind, J.: AIRS/AMSU/HSB on the aqua mission: Design, science objectives, data products, and processing systems, IEEE Trans. Geosci. Remote S., 41, 253–264, 2003.

Baldridge, A. M., Hook, S. J., Grove, C. I., and Rivera, G.: The ASTER Spectral Library Version 2.0., Remote Sens. Environ., 114, 711–715, 2009.

Crevoisier, C., Nobileau, D., Fiore, A. M., Armante, R., Chédin, A., and Scott, N. A.: Tropospheric methane in the tropics – first year from IASI hyperspectral infrared observations, Atmos. Chem. Phys., 9, 6337–6350, doi:10.5194/acp-9-6337-2009, 2009.

Crevoisier, C., Nobileau, D., Armante, R., Crépeau, L., Machida, T., Sawa, Y., Matsueda, H., Schuck, T., Thonat, T., Pernin, J., Scott, N. A., and Chédin, A.: The 2007–2011 evolution of tropical methane in the mid-troposphere as seen from space by MetOp-A/IASI, Atmos. Chem. Phys., 13, 4279–4289, doi:10.5194/acp-13-4279-2013, 2013.

Deeter, M. N., Edwards, D. P., Gille, J. C., and Drummond, J. R.: Sensitivity of MOPITT observations to carbon monoxide in the lower troposphere, J. Geophys. Res., 112, D24306, doi:10.1029/2007JD008929, 2007.

Frankenberg, C., Bergamaschi, P., Butz, A., Houweling, S., Meirink, J. F., Notholt, J., Petersen, A. K., Schrijver, H., Warneke, T., and Aben, I.: Tropical methane emissions: A revised view from SCIAMACHY onboard ENVISAT, Geophys. Res. Lett., 35, L15811, doi:10.1029/2008GL034300, 2008.

Frankenberg, C., Aben, I., Bergamaschi, P., Dlugokencky, E. J., Van Hees, R., Houweling, S., Van der Meer, P., Snel, R., and Tol, P.: Global column-averaged methane mixing ratios from 2003 to 2009 as derived from sciamachy: Trends and variability, J. Geophys. Res., 116, D04302, doi:10.1029/2010JD014849, 2011.

Goddard Earth Sciences Data and Information Services Center (DISC): AIRS V6 CH_4 product, available at: http://mirador.gsfc.nasa.gov/cgi-bin/mirador/presentNavigation.pl?tree=project&project=AIRS, last access: 2 August 2016.

GOSAT user interface gateway (GUIG): GOSAT TANSO-FTS TIR Level 2 CH_4 product, available at: https://data.gosat.nies.go.jp/GosatUserInterfaceGateway/guig/GuigPage/open.do, last access: 24 May 2014.

Illingworth, S. M., Allen, G., Newman, S., Vance, A., Marenco, F., Harlow, R. C., Taylor, J., Moore, D. P., and Remedios, J. J.: Atmospheric composition and thermodynamic retrievals from the ARIES airborne FTS system – Part 1: Technical aspects and simulated capability, Atmos. Meas. Tech., 7, 1133–1150, doi:10.5194/amt-7-1133-2014, 2014.

IPCC: Climate Change 2013: The Physical Science Basis, Working Group I Contribution to the Fifth Assessment Report of the Intergovernmental Panel on Climate Change, edited by: Stocker, T. F., Qin, D., Plattner, G.-K., Tignor, M., Allen, S. K., Boschung, J., Nauels, A., Xia, Y., Bex, V., and Midgey, P. M., Cambridge University Press, Cambridge, United Kingdom and New York, NY, USA, 1535 pp., 2013.

Kuze, A., Suto, H., Nakajima, M., and Hamazaki, T.: Thermal and near infrared sensor for carbon observation Fourier-transform spectrometer on the Greenhouse Gases Observing Satellite for greenhouse gases monitoring, Appl. Optics, 48, 6716–6733, 2009.

Kuze, A., Suto, H., Shiomi, K., Urabe, T., Nakajima, M., Yoshida, J., Kawashima, T., Yamamoto, Y., Kataoka, F., and Buijs, H.: Level 1 algorithms for TANSO on GOSAT: processing and on-orbit calibrations, Atmos. Meas. Tech., 5, 2447–2467, doi:10.5194/amt-5-2447-2012, 2012.

Maksyutov, S., Patra, P. K., Onishi, R., Saeki, T., and Nakazawa, T.: NIES/FRCGC global atmospheric tracer transport model: Description, validation, and surface sources and sinks inversion, Journal of the Earth Simulator, 9, 3–18, 2008.

Parker, R., Boesch, H., Cogan, A., Fraser, A., Feng, L., Palmer, P. I., Messerschmidt, J., Deutscher, N., Griffith, D. W. T., Notholt, J., Wennberg, P. O., and Wunch, D.: Methane observations from the Greenhouse Gases Observing SATellite: Comparison to ground-based TCCON data and model calculations, Geophys. Res. Lett., 38, L15807, doi:10.1029/2011GL047871, 2011.

Payne, V. H., Clough, S. A., Shephard, M. W., Nassar, R., and Logan, J. A.: Information-centered representation of retrievals with limited degrees of freedom for signal: Application to methane from the tropospheric emission spectrometer, J. Geophys. Res., 114, D10307, doi:10.1029/2008JD010155, 2009.

Razavi, A., Clerbaux, C., Wespes, C., Clarisse, L., Hurtmans, D., Payan, S., Camy-Peyret, C., and Coheur, P. F.: Characterization of methane retrievals from the IASI space-borne sounder, Atmos. Chem. Phys., 9, 7889–7899, doi:10.5194/acp-9-7889-2009, 2009.

Rodgers, C. D.: Inverse methods for atmospheric sounding: Theory and Practic, World Scientific Publishing Co. Pte. Ltd, Singapore, ISBN-10: 981-02-2740-X, 2000.

Rodgers, C. D. and Connor, B. J.: Intercomparison of remote sounding instruments, J. Geophys. Res., 108, 4116, doi:10.1029/2002JD002299, 2003.

Saeki, T., Saito, R., Belikov, D., and Maksyutov, S.: Global high-resolution simulations of CO_2 and CH_4 using a NIES transport model to produce a priori concentrations for use in satellite data retrievals, Geosci. Model Dev., 6, 81–100, doi:10.5194/gmd-6-81-2013, 2013.

Saitoh, N., Imasu, R., Ota, Y., and Niwa, Y.: CO_2 retrieval algorithm for the thermal infrared spectra of theGreenhouse Gases Observing Satellite: Potential of retrieving CO_2 vertical profile from high-resolution FTS sensor, J. Geophys. Res., 114, D17305, doi:10.1029/2008JD011500, 2009.

Saitoh, N., Touno, M., Hayashida, S., Imasu, R., Shiomi, K., Yokota, T., Yoshida, Y., Machida, T., Matsueda, H., and Sawa, Y.: Comparisons between X_{CH_4} from GOSAT Shortwave and Thermal Infrared Spectra and Aircraft CH_4 Measurements over Guam, Scientific Online Letters on the Atmosphere, 8, 145–149, doi:10.2151/sola.2012-036, 2012.

Saitoh, N., Kimoto, S., Sugimura, R., Imasu, R., Kawakami, S., Shiomi, K., Kuze, A., Machida, T., Sawa, Y., and Matsueda, H.: Algorithm update of the GOSAT/TANSO-FTS thermal infrared CO_2 product (version 1) and validation of the UTLS CO_2 data using CONTRAIL measurements, Atmos. Meas. Tech., 9, 2119–2134, doi:10.5194/amt-9-2119-2016, 2016.

Schepers, D., Guerlet, S., Butz, A., Landgraf, J., Frankenberg, C., Hasekamp, O., Blavier, J. F., Deutscher, N. M., Griffith, D. W. T., Hase, F., Kyro, E., Morino, I., Sherlock, V., Sussmann, R., and Aben, I.: Methane retrievals from Greenhouse Gases Observing Satellite (GOSAT) shortwave infrared measurements: Performance comparison of proxy and physics retrieval algorithms, J. Geophys. Res., 117, D10307, doi:10.1029/2012jd017549, 2012.

Tans, P. P.: The atmospheric buildup rate for carbon is based on measurements of CO_2 at Mauna Loa obtained by the NOAA Earth System Research Laboratory, available at: ftp://aftp.cmdl.noaa.gov/products/trends/co2/co2_gr_mlo.txt, www.esrl.noaa.gov/gmd/ccgg/trends/ (last access: 5 October 2015), 2009.

Wecht, K. J., Jacob, D. J., Wofsy, S. C., Kort, E. A., Worden, J. R., Kulawik, S. S., Henze, D. K., Kopacz, M., and Payne, V. H.: Validation of TES methane with HIPPO aircraft observations: implications for inverse modeling of methane sources, Atmos. Chem. Phys., 12, 1823–1832, doi:10.5194/acp-12-1823-2012, 2012.

Worden, J., Kulawik, S., Frankenberg, C., Payne, V., Bowman, K., Cady-Peirara, K., Wecht, K., Lee, J.-E., and Noone, D.: Profiles of CH_4, HDO, H_2O, and N_2O with improved lower tropospheric vertical resolution from Aura TES radiances, Atmos. Meas. Tech., 5, 397–411, doi:10.5194/amt-5-397-2012, 2012.

Xiong, X., Barnet, C., Maddy, E., Sweeney, C., Liu, X., Zhou, L., and Goldberg, M.: Characterization and validation of methane products from the Atmospheric Infrared Sounder (AIRS), J. Geophys. Res., 113, G00A01, doi:10.1029/2007JG000500, 2008.

Xiong, X., Barnet, C., Maddy, E., Wei, J., Liu, X., and Pagano, T. S.: Seven Years' Observation of Mid-Upper Tropospheric Methane from Atmospheric Infrared Sounder, Remote Sens., 2, 2509–2530, 2010a.

Xiong, X., Barnet, C. D., Zhuang, Q., Machida, T., Sweeney, C., and Patra, P. K.: Mid-upper tropospheric methane in the high Northern Hemisphere: Spaceborne observations by AIRS, aircraft measurements, and model simulations, J. Geophys. Res., 115, D19309, doi:10.1029/2009JD013796, 2010b.

Xiong, X., Barnet, C., Maddy, E. S., Gambacorta, A., King, T. S., and Wofsy, S. C.: Mid-upper tropospheric methane retrieval from IASI and its validation, Atmos. Meas. Tech., 6, 2255–2265, doi:10.5194/amt-6-2255-2013, 2013.

Xiong, X., Weng, F., Liu, Q., and Olsen, E.: Space-borne observation of methane from atmospheric infrared sounder version 6: validation and implications for data analysis, Atmos. Meas. Tech. Discuss., 8, 8563–8597, doi:10.5194/amtd-8-8563-2015, 2015.

Yokota, T., Yoshida, Y., Eguchi, N., Ota, Y., Tanaka, T., Watanabe, H., and Maksyutov, S.: Global Concentrations of CO_2 and CH_4 Retrieved from GOSAT: First Preliminary Results, SOLA, 5, 160–163, 2009.